RESEARCH ARTICLE | APRIL 29 2009

Sputtered In_2O_3 and ITO thin films containing zirconium ⊘

T. A. Gessert; Y. Yoshida; C. C. Fesenmaier; T. J. Coutts

🔴 Check for updates

View Online   Export Citation

Articles You May Be Interested In

High-performance a-ITZO TFTs with high bias stability enabled by self-aligned passivation using a-GaO$_x$

Appl. Phys. Lett. (November 2022)

Improved performance and stability of In-Sn-Zn-O thin film transistor by introducing a meso-crystalline ZrO$_2$ high-k gate insulator

J. Vac. Sci. Technol. A (February 2019)

Low temperature processing of indium-tin-zinc oxide channel layers in fabricating thin-film transistors
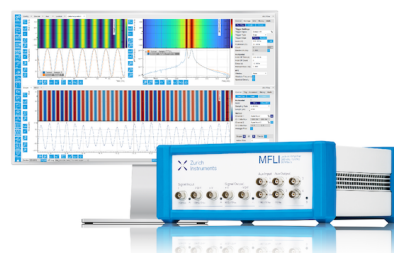
J. Vac. Sci. Technol. B (February 2011)

Sputtered In$_2$O$_3$ and ITO thin films containing zirconium

T. A. Gessert,[a)] Y. Yoshida, C. C. Fesenmaier, and T. J. Coutts
National Renewable Energy Laboratory, 1617 Cole Blvd., Golden, Colorado 80401, USA

Additions of Zr to In$_2$O$_3$ (IO) and In$_2$O$_3$:SnO$_2$ (ITO) sputtered thin films are studied. We find that Zr allows IO-based films to maintain optical transparency as oxygen partial pressure in the sputter ambient decreases, and it also maintains high carrier concentration as the oxygen partial pressure increases. Applying this guidance could indicate pathways to improve film properties in large-area deposition systems. We also find that for films deposited at optimum oxygen partial pressure, the optical transparency of the IO-based films improves as Zr is added, especially in the near-infrared spectral region. Analysis of these films using Drude theory approximations indicate that optical improvement is due to an increase in dielectric permittivity caused by Zr addition. We propose that controlling dielectric permittivity may be an important strategy in improving other transparent conducting oxides (TCOs), as well as indicative of an important pathway to developing new TCOs. © *2009 American Institute of Physics*. [DOI: 10.1063/1.3116542]

I. INTRODUCTION

Doped In$_2$O$_3$ (IO) films represent some of the highest-quality transparent conducting oxides (TCOs) presently available. Reasons include its ability to maintain high mobility at high carrier concentration and low optical absorption. IO films can be doped using several group IVA and IVB dopants, including Ti, Zr (IZrO), and Sn (In$_2$O$_3$:SnO$_2$) (ITO).[1] However, most reports suggest that the optimal balance between electrical and optical quality is produced with Sn doping.[2] High-quality ITO films can be produced by magnetron sputtering using substrate temperatures of 250°–350 °C and an ambient in which the oxygen partial pressure is controlled to yield a slight oxygen deficiency in the film. However, when the sputter ambient becomes too oxygen deficient, the optical transparency of the film decreases. The challenge during ITO deposition is to incorporate enough oxygen to produce films with high transparency and optimal electrical properties. In production coating systems, this critical balance of oxygen must be maintained over a large deposition area, and it is often adjusted for variations in target use, seasonal changes, and maintenance activities.

Our recent investigations have identified a method to produce films that are similar to ITO but are less sensitive to variations in the oxygen-containing deposition ambient. We have used IO and ITO ceramic sputtering targets that contain a small amount of Zr to produce sputtered films on barium borosilicate glass substrates. Electrical and optical analyses of these films reveal that an ~0.5 at. % addition of Zr to ITO (referred to as ITZO) allows fabrication of low-resistance films at higher oxygen partial pressure and fabrication of higher optical-transmission films at lower oxygen partial pressure. The improved optical transmission is especially obvious in the near-infrared (NIR) spectral region. We believe these benefits may embody advantages for large-area

ITO film production and could point the way toward similar benefits in other TCOs such as those based on ZnO, SnO$_2$, CdO, and mixed alloys.

II. EXPERIMENTAL

Films were prepared using radio-frequency magnetron sputtering at 13.56 MHz in a sputter-down configuration from 2 in. planar targets of 99.99% purity. The source-substrate separation was ~1.27 cm. Doped targets were fabricated by CERAC, Inc. (Milwaukee, WI) and were produced by hot pressing followed by firing in oxygen at 760 °C. The undoped IO target was produced by Pure Tech (Brewster, NY) and was 99.99% pure. The four target compositions compared in this study are shown in Table I. Film deposition was performed in a Unifilm Technologies sputtering system that is capable of automated control of both substrate orbit and rotary motion to enhance deposit uniformity. Base pressures of $5 \times 10^{-8} - 2 \times 10^{-7}$ torr were established using a cryopump (maximum specified throughput $= 8.9$ torr l s^{-1}, Ar) prior to each deposition. Ultra-high-purity argon (99.999%) and oxygen (99.995%) were used as the sputtering gases. Gas flows (and partial pressure ratio) were set using needle valves prior to throttling to the sputtering pressure of 10 mtorr, which was measured with a

TABLE I. Nominal composition for each sputtering target used in this study. Dopant concentration was calculated assuming specified target compositions.

Target	Specified target composition (wt %)			Dopant concentration (at. %)	
	In$_2$O$_3$	SnO$_2$	ZrO$_2$	Sn	Zr
IO	100	0	0	0	0
IZrO	91	0	9	0	3.93
ITO	91	9	0	3.29	0
ITZO	90	9	1	3.27	0.49

a)Electronic mail: tim_gessert@nrel.gov.

temperature-compensated capacitive manometer. The ratio of oxygen to argon pressure in the sputter ambient is described as $O_2\%$ using the following relation:

$$O_2\% = \{P(O_2)/[P(Ar) + P(O_2)]\}100, \qquad (1)$$

where $P(O_2)$ and $P(Ar)$ are the oxygen and argon pressures measured with an ion gauge before throttling. Note, because the ionization efficiency of Ar is higher than O_2, the *absolute* $O_2\%$ in the ambient will be higher than the *relative* $O_2\%$ indicated by Eq. (1). Sputtering was conducted at constant power of 80 W, and films were produced with thicknesses from ∼100 to ∼1200 nm.

Corning 7059 glass substrates were cleaned using a 5% solution of 18 MΩ de-ionized water and Citranox in an ultrasonic bath for 10 min, followed by rinsing in de-ionized water, spin rinsing to an output water resistivity of 12 MΩ and spin drying. Substrates were placed on a rotatable heater (boron-nitride element) operating at a constant voltage. Depositions were performed at substrate temperatures of 120°–420 °C. The substrate temperature was calibrated in vacuum by placing a 0.32-cm-thick Al block with an embedded thermocouple at the substrate position and allowing the block to equilibrate for 2 h. Following deposition, the samples were maintained in the sputtering ambient and temperature for 1 h, after which the gases and the heater were shut off and the substrate was allowed to cool under vacuum for 1 h. This postdeposition procedure was found to be necessary to achieve reproducibility of film electrical parameters.

The thickness of the ∼200–1200 nm films was measured using stylus profilometry (Veeco Dektak 3), and the 100–200 nm films were measured using ellipsometry (Rudolph Research Type 43702–200E). Optical measurements were performed using a spectrophotometer (Varian Cary 5G) in the wavelength range of 300–2500 nm. The film resistivity, mobility, and carrier concentration were obtained at room temperature from Hall analysis using the van der Pauw method (BioRad HL5500 System).

Spectroscopic ellipsometry (SE) measurements were performed to analyze dielectric constants using a J.A. Woollam M-2000 rotating compensator ellipsometer at three angles of incidence (55°, 60°, and 65°) in the spectral range of 800–1700 nm. The data were analyzed using a three-layer optical model consisting of surface roughness, a graded TCO film, and a glass substrate. The TCO film was represented by a Drude oscillator to model free-carrier absorption at long wavelengths and by a pole to model dispersion due to absorption at higher energies outside the spectral range. The oscillator parameters were allowed to vary independently at the top and bottom of the TCO film and were connected by a multinode linear grading. Surface roughness was modeled as a Bruggeman effective medium approximation of a 50% mixture of voids and TCO material. Layer thicknesses, grading, and optical constant parameters were fit simultaneously over multiple angles and wavelengths for each sample.

TABLE II. Representative deposition parameters and resulting electrical properties for IO-based films fabricated during this study. For each film type, electrical properties are indicated for both a high and low $O_2\%$ ambient condition.

Run#	Temp. (°C)	$O_2\%$ (high/low)	$O_2\%$ (%)	Mobility ($cm^2 V^{-1} s^{-1}$)	CC (cm^{-3})	Res. (Ω cm)
IO-43	300	High	2.00	33	5×10^{18}	4×10^{-2}
IO-4	350	Low	1.20	20	2×10^{19}	2×10^{-2}
IZrO-1	350	High	0.50	15	4×10^{19}	1×10^{-2}
IZrO-27	350	Low	0.00	11	4×10^{20}	1×10^{-3}
ITO-4	350	High	0.32	37	7×10^{20}	2×10^{-4}
ITO-5	350	Low	0.27	25	1×10^{21}	2×10^{-4}
ITZO-5	350	High	0.63	35	8×10^{20}	2×10^{-4}
ITZO-3	350	Low	0.36	27	1×10^{21}	3×10^{-4}

III. RESULTS

A. Electrical properties of IO, ITO, IZrO, and ITZO films

The material properties of nearly all TCO films are known to demonstrate significant dependence on substrate temperature and $O_2\%$. Previous studies with IO-based materials indicated that optimum material properties are produced at substrate temperatures between 200 and 400 °C.[3,4] At these deposition temperatures, $O_2\%$ is typically optimized at ∼0.3%.[5] Table II shows that results from this work are consistent with these previous studies. The table also provides an indication of material properties for films deposited in a relatively "low" versus "high" $O_2\%$ ambient. Here low and high $O_2\%$ represents the approximate end points of the optimum range of $O_2\%$ for each film type. For these studies, high $O_2\%$ leads to higher mobility and lower carrier concentration, whereas low $O_2\%$ ambient produces lower mobility and higher carrier concentration. Because of the importance of high mobility and low carrier concentration to reduce free-carrier absorption, TCO films are often optimized in the high $O_2\%$ range. For this study, the more important benefit of controlling film electrical properties through $O_2\%$ is that one can produce pairs of ITO and ITZO films that demonstrate nearly identical electrical properties. This allows the effect of Zr on optical properties to be assessed separately from the effect that mobility and carrier concentration have on optical properties (i.e., Drude theory expectations).[6]

Table II shows that minimum resistivity in IO films results from deposition conditions that produce a carrier concentration in the range of 10^{19} cm^{-3} and mobility in the range of 20 $cm^2 V^{-1} s^{-1}$. The reason for low carrier concentration is likely because donors related either directly or indirectly to oxygen vacancies are not as effective as the group IV substitutional donors (i.e., Sn or Zr). The mobility for IO is consistent with other reports, as well as with other undoped TCO thin films.[7] In contrast, ITO films produced during this study had carrier concentrations of (∼7–15) $\times 10^{20}$ cm^{-3}, and the highest-mobility ITO film demonstrated carrier concentration and mobility of 4.4 $\times 10^{20}$ cm^{-3} and 42.5 $cm^2 V^{-1} s^{-1}$, respectively.

IZrO films demonstrated reasonable direct current electrical properties although poorer than the ITO films. Typical
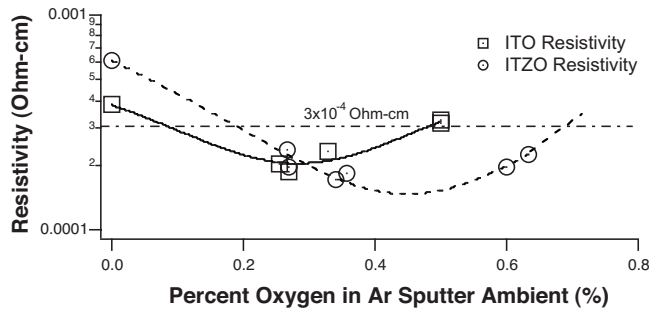
FIG. 1. Comparison of the electrical properties of ITO and ITZO films deposited at optimal temperature and O_2%. Because ITZO films retain low resistivity at higher oxygen partial pressure, ITZO films can be optimized within a process window that includes higher O_2%.

carrier concentrations were $(\sim 0.2-4) \times 10^{20}$ cm^3 with mobilities of $\sim 7-15$ cm^2 V^{-1} s^{-1}. A higher carrier concentration could be expected for the IZrO films compared to the ITO films because the atomic percent of Zr is higher in the IZrO target than Sn in the ITO target (3.93 at. % versus 3.29 at. %, respectively; see Table I). However, the fact that IZrO films demonstrate higher carrier concentration than the IO films indicates that Zr is an effective donor in IO-based TCOs. The observation that IZrO did not achieve mobility greater than ~ 15 cm^2 V^{-1} s^{-1} differs from historic reports in which mobilities approaching 100 cm^2 V^{-1} s^{-1} are suggested.[1] The lower mobility achieved in this study may result from differences in deposition processes and/or analysis. However, another possibility is that the concentration of ZrO_2 (9 wt % in our target) is excessive and reducing Zr content may lead to increased mobility in IZrO films. Another important difference between ITO and IZrO films is that the electrical properties of IZrO films were found to be much less sensitive to variations in O_2%.[8] This observation will be discussed more fully below.

Electrical properties of ITZO films were found to be nominally identical to ITO films once the effect of O_2% ambient is considered. This is consistent with the observation that Zr is an effective dopant in IO and suggests that a small amount of ZrO_2 (1 wt % ZrO_2) does not perturb significantly the carrier-scattering processes in the predominantly ITO matrix. Similar to ITO, fabrication of ITZO films with high electrical quality required a small addition of oxygen to the sputtering ambient (~ 0.5%). Also, similar to the IZrO films, and as suggested in Table II, we found that the electrical properties of ITZO films can be optimized over a wider range of O_2% than ITO films. Figure 1 shows that the ITZO film maintains a resistivity of $<3 \times 10^{-4}$ Ω cm to O_2% of 0.7%, whereas the ITO film exceeds this resistivity for O_2% >0.5%. This functionality could provide advantages to large-area production of ITO-like films, especially when one considers that variation in O_2% can arise from many sources, including wall and sample outgassing, leakage, and seasonal humidity variations.[8] As will be shown below, this advantage is leveraged when the optical benefits of Zr addition to ITO are considered.

B. Optical properties of IO, ITO, IZrO, and ITZO films

Figure 2 compares the optical transparency of IO, ITO, IZrO, and ITZO films deposited in pure Ar. These films were
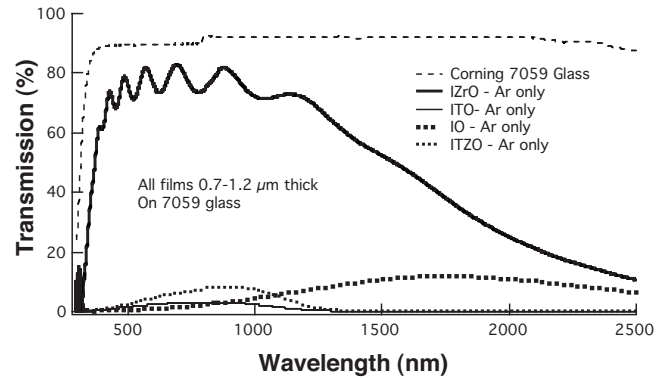

FIG. 2. Figure compares spectral transmission of IZrO, ITO, IO, and ITZO films. All films were deposited in pure Ar. The carrier concentration and mobility of the IZrO film is 2×10^{20} cm^3 and 20 cm^2 V^{-1} s^{-1}, respectively. All films are $0.7-1.2$ μm thick.

produced to be thicker ($0.7-1.2$ μm) than is typical for many applications to enhance differences in optical transmission. The poor transmission demonstrated by most of the films (<5%) is consistent for TCO films sputtered at high temperature in an Ar-only ambient with low base pressure of other impurities (base pressure for this study is $\sim 5 \times 10^{-8}$ torr). In contrast, Fig. 2 shows that the IZrO film deposited in pure Ar demonstrates very high transparency (~ 80%). This is true even though this target had been used for numerous prior depositions; therefore, it is unlikely that the higher transmission is due to high (but metastable) oxygen concentration near the target surface. This difference in transmission suggests that the Zr either facilitates oxygen incorporation into the depositing films or changes the material properties such that less oxygen is required to achieve high transparency. Figure 3 compares a thinner IZrO film (~ 0.1 μm) produced in pure Ar with two ITO films produced in optimal O_2%. One of the ITO films shown in Fig. 3 was produced using the same target used to produce the ITO target shown in Fig. 2, and the other was produced by a commercial vendor. The comparison shows that the IZrO film sputtered in pure Ar is of comparable optical quality to
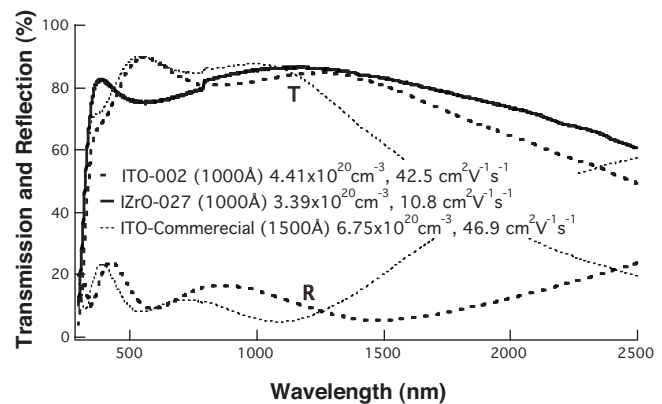

FIG. 3. Figure compares spectral transmission of an IZrO film deposited in pure Ar, an ITO film of similar thickness produced in an optimal Ar/O_2 ambient, and an ITO film produced by a commercial vendor. Reflection is shown for ITO films but is not available for the IZrO film. Comparison illustrates that the IZrO film deposited in pure Ar is of good optical quality even when compared to high-quality ITO films.
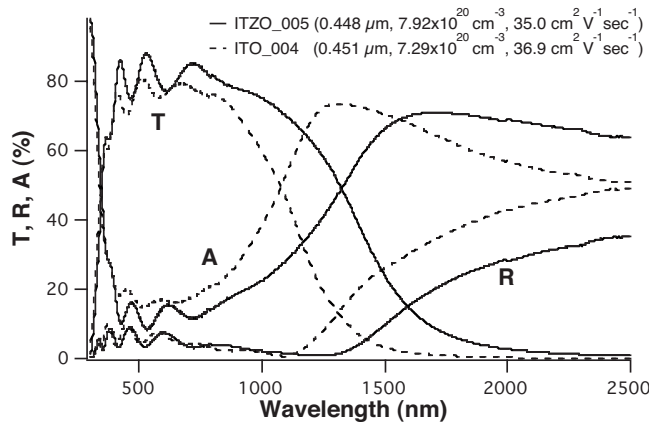
FIG. 4. Comparison of optical reflection, transmission, and absorption of ITZO and ITO films deposited in a high O$_2$% ambient. Note that both films demonstrate a carrier concentration of ~7×10^{20} cm^{-3} and similar mobilities.

both of the other "optimal" ITO films, suggesting that IZrO may have applications in which films grown without oxygen are preferred.

Based on the indications that Zr is both a reasonable *n*-type dopant for IO and that IZrO can maintain high film transparency at low O$_2$%, ITZO films were produced to determine if the optical benefits observed for IZrO could be engineered into a film with an electrical quality more consistent with ITO. Figure 4 shows an ITZO and ITO film that was produced using high O$_2$% in the sputtering ambient, while Fig. 5 shows a similar pair of films produced in a low O$_2$% ambient. Note that these figures compare films that are both of similar thickness and electrical properties (i.e., carrier concentrations and mobility, measured using room-temperature Hall measurements). By selecting ITO and ITZO films with this high degree of similarity, differences due to free-carrier absorption can be minimized.[6] The comparisons show that the ITZO films demonstrate higher transmission than the ITO film in both the visible (~500–700 nm) and NIR spectral region. It is also noted that the difference in NIR transmission of the ITZO film is even greater for the films with lower carrier concentration shown in Fig. 4. Our suggested reasons for these observations are discussed below.
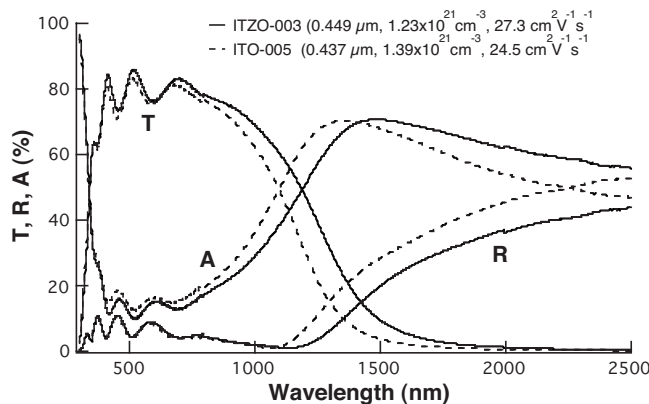

FIG. 5. Comparison of optical reflection, transmission, and absorption of ITZO and ITO films deposited in a low O$_2$% ambient. Note that both films demonstrate a carrier concentration of ~1×10^{21} cm^{-3} and similar mobilities.
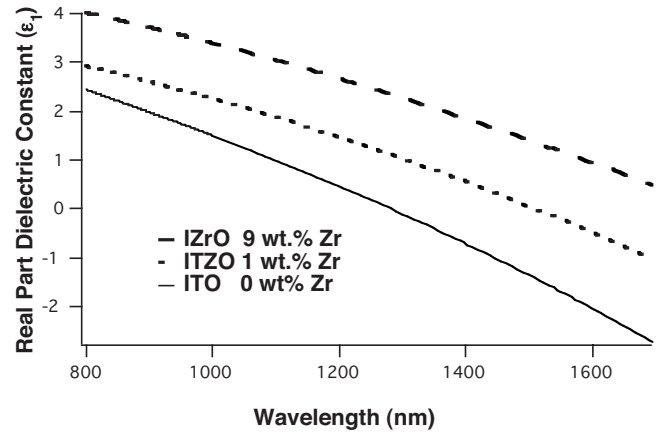

FIG. 6. SE analysis of ε_1 vs wavelength. Data were modeled for the region at the bottom of the film (film/glass interface). Because the plasma wavelength is defined at the point at which $\varepsilon_1=0$, figure shows that λ_p increases significantly as Zr is added to the film.

C. SE

Drude theory is usually adequate to explain the optical and electrical properties of TCOs. However, the difference in optical transmission shown in Figs. 4 and 5 for films with similar carrier concentration and mobility suggests that the details of free-electron absorption as suggested by Drude theory require closer inspection. Figure 6 shows SE analysis indicating the spectral variation for the real part of the dielectric coefficient (ε_1) in the spectral range of 800–1700 nm. The ITO and ITZO films shown in Fig. 6 are the same films shown in Fig. 4 and have very similar carrier concentration. The SE data were fitted using a linear graded-layer model with five steps between nodes (two or three nodes incorporated), in which the end points were fixed and the complex dielectric coefficient within the central region was allowed to vary. The data shown in Fig. 6 represent ε_1 at the bottom of the respective film stacks (i.e., the location near the TCO/glass interface). The SE analysis shows that as Zr is added to the IO host material, ε_1 increases within the wavelength range probed. This overall increase in ε_1 with Zr content in this spectral range remains true, regardless of the film depth at which ε_1 is analyzed.

IV. DISCUSSION

The results above indicate that addition of Zr to IO-based TCOs can provide the following benefits compared to ITO: (1) for films deposited in similar O$_2$% ambient, Zr-containing films maintain higher carrier concentration at higher O$_2$%; (2) for films deposited in similar O$_2$% ambient, Zr-containing films maintain higher transparency at reduced O$_2$%; and (3) Zr-containing films demonstrate higher visible and infrared transparency at optimum O$_2$%. The combination of the first two benefits presents a compelling pathway toward the production of ITO-like films with a wider window for process optimization and reproducibility. The third observation suggests that the addition of Zr has produced a fundamental alteration to the ITO material and that it may be possible to exploit this alteration to improve the performance of TCOs, in general.

It is assumed in most TCO investigations that the dielectric permittivity does not change appreciably as the TCO is altered by dopant addition and/or material processing. However, it is well established that *for dielectric oxides*, permittivity can be increased by the addition of higher-permittivity oxides such as ZrO_2 and HfO_2.[9] It is also known that the permittivity of dielectric oxides increases rapidly with even small additions of a higher-permittivity constituent.[10] Examining the Drude theory equations that have been found to describe effectively TCO optical and electrical properties, one can obtain the following relationships for the frequency (ω) dependence for the real (ε_1) and imaginary (ε_2) parts of the complex permittivity:

$$\varepsilon_1(\omega) = \varepsilon_\infty - \frac{ne^2}{\varepsilon_o m^* \omega^2}, \tag{2}$$

$$\varepsilon_2(\omega) = \frac{ne^2}{\varepsilon_o m^* \omega^3 \tau}, \tag{3}$$

where ε_∞ is the high-frequency permittivity for a particular material, ε_o is the permittivity of free space, m^* is the effective mass of the carriers, n is the carrier density, e is the electronic charge, and τ is the relaxation time between scattering events. $\varepsilon_1(\omega)$ indicates the ability of the constituents of the material (i.e., ion cores, electrons) to become polarized in the presence of electromagnetic oscillations. The plasma frequency (ω_p) is obtained at the frequency where $\varepsilon_1(\omega)$ in Eq. (2) equals zero,

$$\omega_p = \sqrt{\frac{ne^2}{\varepsilon_o \varepsilon_\infty m^*}}. \tag{4}$$

The plasma wavelength (λ_p) is

$$\lambda_p = \frac{c}{2\pi\omega_p} = \frac{c}{2\pi} \sqrt{\frac{\varepsilon_o \varepsilon_\infty m^*}{ne^2}}, \tag{5}$$

where c is the speed of light.

Equations (2)–(5) provide a framework to interpret the results shown in Figs. 4–6. In Fig. 6, SE shows that $\varepsilon_1(\omega)$ increases systematically as Zr is added to the ITO matrix. Equation (2) states that $\varepsilon_1(\omega)$ can increase at a given frequency by increasing either ε_∞ or m^* or both. However, because Fig. 6 shows $\varepsilon_1(\omega)$ is not approaching a similar value at short wavelength for films with different amounts of Zr, we believe that the difference in $\varepsilon_1(\omega)$ is more consistent with ε_∞ increasing with Zr content rather than m^*. The long-wavelength end in Fig. 6 shows that the increase in ε_∞ causes λ_p [i.e., the wavelength at which $\varepsilon_1(\omega)=0$] to increase from $\sim$1300 nm for ITO to $\sim$1550 nm for ITZO ($\sim$1 wt % ZrO_2) and still longer values for IZrO ($\sim$9 wt % ZrO_2). As λ_p increases, optical absorption and reflection due to electrons coupling more efficiently to the electromagnetic field (i.e., plasma resonance) will move to longer wavelengths. This will lead to improvement in NIR transmission of ITZO films in Figs. 4 and 5 relative to the lower-permittivity ITO films.

The observation that the films shown in Fig. 4 ($n=7-8 \times 10^{20}$ cm^{-3}) demonstrate a greater shift in λ_p compared to the films shown in Fig. 5 ($n=1.3 \times 10^{21}$ cm^{-3}) is predicted by Eq. (5) and can be illustrated by first differentiating by ε_∞ and then by n,

$$\frac{\partial \lambda_p}{\partial \varepsilon_\infty} = \frac{c}{4\pi} \sqrt{\frac{\varepsilon_o m^*}{\varepsilon_\infty ne^2}} = \frac{\lambda_p}{2\varepsilon_\infty} \tag{6}$$

$$\frac{\partial}{\partial n}\left(\frac{\partial \lambda_p}{\partial \varepsilon_\infty}\right) = -\frac{c}{8\pi} \sqrt{\frac{\varepsilon_o m^*}{\varepsilon_\infty n^3 e^2}} = -\frac{\lambda_p}{4\varepsilon_\infty n}. \tag{7}$$

Equation (6) indicates that although λ_p increases with ε_∞ (differential is positive), the rate of change diminishes with increasing ε_∞. Therefore, Drude theory predicts—and this study has shown—that a significant NIR shift in λ_p should be realized for relatively small increases in permittivity. As is well established, Eq. (7) indicates that λ_p decreases with n (differential is negative) and, further, that the rate of change in λ_p diminishes with increasing n for any given value of ε_∞. This indicates that for any two values of ε_∞ (i.e., ε_∞ values associated with ITO versus ITZO), λ_p will change less for films with larger values of n; thus, this explains the difference observed for the λ_p shift between Figs. 4 and 5.

V. CONCLUSIONS

Although replacing Sn with Zr as a dopant has not produced films with electrical properties superior to ITO, we have found that IZrO films with very high optical quality can be deposited at high temperature in pure Ar. This attribute may provide advantages in certain applications in which excess oxygen in the sputter ambient must be avoided. Because Zr additions also allow high-quality IO-based films to be produced over a wider range of oxygen partial pressure, Zr additions may also provide advantages for large-area production in which accurate control of oxygen partial pressure uniformity is difficult.

An even more intriguing result is that dielectric permittivity increases when Zr is added to an IO-based TCO. This permittivity increase can be significant even for small values of Zr ($\sim$1 wt % ZrO_2), and it is consistent with observations of ZrO_2 (and HfO_2) additions into SiO_2. The increase in ε_∞ as Zr is added can shift λ_p to a longer wavelength and make it possible to improve NIR transmission significantly without altering the material parameters that relate to carrier concentration or mobility. Because it may be much easier to increase ε_∞ in a TCO than it is to improve mobility, this insight may have significant ramifications in identifying TCO materials with improved quality.

[1] R. Groth, Phys. Status Solidi **14**, 69 (1966).
[2] K. L. Chopra, S. Major, and D. K. Pandya, Thin Solid Films **102**, 1 (1983).
[3] Y. Qu, T. A. Gessert, T. J. Coutts, and R. Noufi, J. Vac. Sci. Technol. A **12**, 1507 (1994).
[4] A. L. Leenheer, J. D. Perkins, M. van Hest, J. J. Berry, R. P. O'Hayre, and D. S. Ginley, Phys. Rev. B **77**, 115215 (2008).

[5]Y. Yoshida, D. M. Woods, T. A. Gessert, and T. J. Coutts, Appl. Phys. Lett. **84**, 2097 (2004).

[6]T. Coutts, D. L. Young, and X. Li, MRS Bull. **25**, 58 (2000).

[7]J. N. Duenow, T. A. Gessert, D. M. Wood, T. M. Barnes, B. To, and T. J. Coutts, J. Vac. Sci. Technol. A **25**, 955 (2007).

[8]T. A. Gessert, Y. Yoshida, and T. J. Coutts, U.S. Patent Application No. 11/718,628 (4 May 2007).

[9]G. D. Wilk, R. M. Wallace, and J. M. Anthony, J. Appl. Phys. **89**, 5243 (2001).

[10]G. Lucovsky and G. B. Rayner, Jr., Appl. Phys. Lett. **77**, 2912 (2000).